

# Transverse momentum and rapidity dependence of HBT correlations in Au+Au collisions at $\sqrt{s_{NN}} = 62.4$ and 200 GeV

B.B.Back<sup>1</sup>, M.D.Baker<sup>2</sup>, M.Ballintijn<sup>4</sup>, D.S.Barton<sup>2</sup>, R.R.Betts<sup>6</sup>, A.A.Bickley<sup>7</sup>, R.Bindel<sup>7</sup>, A.Budzanowski<sup>3</sup>,  
W.Busza<sup>4</sup>, A.Carroll<sup>2</sup>, Z.Chai<sup>2</sup>, M.P.Decowski<sup>4</sup>, E.García<sup>6</sup>, T.Gburek<sup>3</sup>, N.George<sup>1,2</sup>, K.Gulbrandsen<sup>4</sup>, S.Gushue<sup>2</sup>,  
C.Halliwell<sup>6</sup>, J.Hamblen<sup>8</sup>, M.Hauer<sup>2</sup>, G.A.Heintzelman<sup>2</sup>, C.Henderson<sup>4</sup>, D.J.Hofman<sup>6</sup>, R.S.Hollis<sup>6</sup>, R.Hotyński<sup>3</sup>,  
B.Holzman<sup>2</sup>, A.Iordanova<sup>6</sup>, E.Johnson<sup>8</sup>, J.L.Kane<sup>4</sup>, J.Katzy<sup>4,6</sup>, N.Khan<sup>8</sup>, W.Kucewicz<sup>6</sup>, P.Kulinich<sup>4</sup>,  
C.M.Kuo<sup>5</sup>, W.T.Lin<sup>5</sup>, S.Manly<sup>8</sup>, D.McLeod<sup>6</sup>, A.C.Mignerey<sup>7</sup>, R.Nouicer<sup>6</sup>, A.Olszewski<sup>3</sup>, R.Pak<sup>2</sup>, I.C.Park<sup>8</sup>,  
H.Pernegger<sup>4</sup>, C.Reed<sup>4</sup>, L.P.Remsberg<sup>2</sup>, M.Reuter<sup>6</sup>, C.Roland<sup>4</sup>, G.Roland<sup>4</sup>, L.Rosenberg<sup>4</sup>, J.Sagerer<sup>6</sup>, P.Sarin<sup>4</sup>,  
P.Sawicki<sup>3</sup>, H.Seals<sup>2</sup>, I.Sedykh<sup>2</sup>, W.Skulski<sup>8</sup>, C.E.Smith<sup>6</sup>, M.A.Stankiewicz<sup>2</sup>, P.Steinberg<sup>2</sup>, G.S.F.Stephans<sup>4</sup>,  
A.Sukhanov<sup>2</sup>, J.-L.Tang<sup>5</sup>, M.B.Tonjes<sup>7</sup>, A.Trzupek<sup>3</sup>, C.Vale<sup>4</sup>, G.J.van Nieuwenhuizen<sup>4</sup>, S.S.Vauryovich<sup>4</sup>,  
R.Verdier<sup>4</sup>, G.I.Verés<sup>4</sup>, E.Wenger<sup>4</sup>, F.L.H.Wolfs<sup>8</sup>, B.Wosiek<sup>3</sup>, K.Woźniak<sup>3</sup>, A.H.Wuosmaa<sup>1</sup>, B.Wysłouch<sup>4</sup>  
(PHOBOS Collaboration)

<sup>1</sup> Argonne National Laboratory, Argonne, IL 60439-4843, USA

<sup>2</sup> Brookhaven National Laboratory, Upton, NY 11973-5000, USA

<sup>3</sup> Institute of Nuclear Physics PAN, Kraków, Poland

<sup>4</sup> Massachusetts Institute of Technology, Cambridge, MA 02139-4307, USA

<sup>5</sup> National Central University, Chung-Li, Taiwan

<sup>6</sup> University of Illinois at Chicago, Chicago, IL 60607-7059, USA

<sup>7</sup> University of Maryland, College Park, MD 20742, USA

<sup>8</sup> University of Rochester, Rochester, NY 14627, USA

(Dated: November 13, 2018)

Two-particle correlations of identical charged pion pairs from Au+Au collisions at  $\sqrt{s_{NN}} = 62.4$  and 200 GeV were measured by the PHOBOS experiment at RHIC. Data for the 15% most central events were analyzed with Bertsch-Pratt and Yano-Koonin-Podgoretskii parameterizations using pairs with rapidities of  $0.4 < y_{\pi\pi} < 1.3$  and transverse momenta  $0.1 < k_T < 1.4$  GeV/c. The Bertsch-Pratt radii  $R_o$  and  $R_\ell$  decrease as a function of pair transverse momentum, while  $R_s$  is consistent with a weaker dependence.  $R_o$  and  $R_s$  are independent of collision energy, while  $R_\ell$  shows a slight increase. The source rapidity  $y_{YKP}$  scales roughly with the pair rapidity  $y_{\pi\pi}$ , indicating strong dynamical correlations.

PACS numbers: 25.75.-q, 25.75.Dw, 25.75.Gz

Recent experimental results from all four experiments at the Relativistic Heavy Ion Collider (RHIC) have concluded that Au+Au collisions at the top RHIC energy ( $\sqrt{s_{NN}} = 200$  GeV) have produced an extremely hot and dense state of matter [1, 2, 3, 4]. This matter may have degrees of freedom that are purely hadronic (“hadronic gas”), purely partonic (“Quark-Gluon Plasma”, QGP), or an admixture of both. Identical-particle correlation measurements (Hanbury-Brown and Twiss, HBT) yield valuable information on the size, shape, duration, and spatiotemporal evolution of the emission source. Because the dynamics of a hadron gas and a QGP are naïvely expected to be quite different, HBT may allow us to discriminate between these three scenarios [5, 6].

Experimentally, the correlation function  $C(\mathbf{q})$  is defined as

$$C(\mathbf{q}) = \frac{P(\mathbf{p}_1, \mathbf{p}_2)}{P(\mathbf{p}_1)P(\mathbf{p}_2)} \quad (1)$$

where  $\mathbf{p}_1$  and  $\mathbf{p}_2$  are the particle four-momenta,  $P(\mathbf{p}_1, \mathbf{p}_2)$  is the probability of a pair being measured with relative four-momentum  $\mathbf{q} = \mathbf{p}_1 - \mathbf{p}_2$ , and  $P(\mathbf{p}_1)$  and  $P(\mathbf{p}_2)$  are the single-particle probabilities. The numerator is determined directly from data, while the de-

nominator is constructed using a standard event-mixing technique.

$C(\mathbf{q})$  can be fit to the Bertsch-Pratt parameterization of a Gaussian source in three dimensions [6, 7, 8],

$$C(\mathbf{q}) = 1 + \lambda e^{-(q_o^2 R_o^2 + q_s^2 R_s^2 + q_\ell^2 R_\ell^2 + 2q_o q_\ell R_o R_\ell)} \quad (2)$$

where  $q_\ell$  is the component of  $\mathbf{q}$  along the beam direction;  $q_o$  is the component along the pair transverse momentum  $\vec{k}_T = \frac{1}{2}(\vec{p}_{T1} + \vec{p}_{T2})$ ; and  $q_s$  is the component orthogonal to the other two. The  $q_o q_\ell$  cross-term vanishes only for symmetric collisions with acceptances centered around midrapidity. The  $\lambda$  parameter represents the correlation strength and is expected to be unity for a completely incoherent source. According to the definitions of  $q_o$  and  $q_s$ ,  $R_o$  probes a mixture of the spatial and temporal extent of the source, while  $R_s$  measures only the spatial component. In the special case of a boost-invariant, transparent, azimuthally symmetric source, the ratio  $R_o/R_s$  may be a good indicator of the duration of the emission of particles from the source. Predictions for this quantity from hydrodynamic and transport models varied by over an order of magnitude [9, 10], but mostly focused on values between 1.5–2.0, while the first results from RHIC at

$\sqrt{s_{NN}} = 130$  GeV indicated a value near unity [11, 12]. A more recent three-dimensional hydrodynamic calculation (including opacity and transverse flow) [13] also was unable to reproduce the experimentally measured values for  $R_o/R_s$ . The results at  $\sqrt{s_{NN}} = 130$  GeV also were consistent with a monotonic increase of  $R_\ell$  from AGS energies ( $\sqrt{s_{NN}} \simeq 2\text{--}5$  GeV), while  $R_o$  and  $R_s$  remained roughly constant. It should be noted that it is possible to fit the experimental data at RHIC to a variety of *ansätze* [14, 15, 16], but the interpretation remains an open question. The wealth of HBT data over a large number of variables and their experimentally-determined systematic dependencies continue to create new challenges for theorists and add yet more pieces to the ‘‘HBT puzzle’’.

The data reported here for Au+Au collisions at  $\sqrt{s_{NN}} = 62.4$  and 200 GeV were collected using the PHOBOS two-arm magnetic spectrometer during RHIC Run IV (2004) and Run II (2001), respectively. Details of the setup have been described previously [17]. The spectrometer arms are each equipped with 16 layers of silicon sensors, providing charged particle reconstruction both outside and inside a 2 T magnetic field. The two symmetric arms and frequent magnetic field polarity reversals allowed for a number of independent cross-checks in the two-particle correlation measurement. A two layer silicon detector covering  $|\eta| < 0.9$  and 25% of the azimuthal angle provided additional information on the position of the primary collision vertex.

The primary event trigger was provided by two sets of 16 scintillator paddle counters, which covered a pseudorapidity range  $3 < |\eta| < 4.5$ . More information on PHOBOS event selection and centrality determination can be found in [18, 19].

The details of the track reconstruction algorithm can be found in [20, 21]. Events with a reconstructed primary vertex position between  $-12 \text{ cm} < z_{vtx} < 10 \text{ cm}$  along the beam direction and  $-0.1 < x_{vtx} < 0.2 \text{ cm}$  and  $-0.05 < y_{vtx} < 0.2 \text{ cm}$  along the transverse directions were selected to optimize vertex-finding precision, track reconstruction efficiency, and momentum resolution. Only particles which traversed the entire spectrometer were used in the analysis. A  $3\sigma$  cut on the distance of closest approach of each reconstructed track with respect to the primary vertex ( $dca_{vtx} < 0.35 \text{ cm}$ ) was used to reject background particles from decays and secondary interactions. The final track selection was based on the  $\chi^2$  probability of a full track fit, taking into account multiple scattering and energy loss. The momentum resolution is  $\Delta p/p \sim 1\%$  after all cuts. Particle identification was based on the truncated mean of the specific ionization loss in the silicon detectors. To identify pions, a cut of three RMS deviations away from the expected mean value of the specific ionization  $\langle dE/dx \rangle$  for pions was applied. This is shown as the region between the solid black lines in Fig. 1. Possible contamination from other particle species was studied using HIJING 1.35 [22] and a GEANT 3.21 [23] simulation of the full detector,

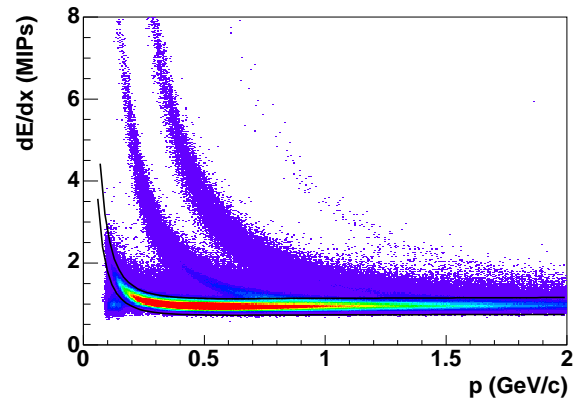


FIG. 1: Distribution of the truncated average energy loss  $\langle dE/dx \rangle$  as a function of reconstructed particle momentum. The region between the solid black lines corresponds to the  $\pm 3\sigma$  cut used to select pions for this analysis.

applying the same reconstruction procedures to Monte Carlo events and data. The contamination from  $K^+K^+$ ,  $K^-K^-$ ,  $pp$ ,  $\bar{p}\bar{p}$ ,  $e^+e^+$ , and  $e^-e^-$  pairs is estimated to be less than 1%; non-identical pairs are estimated to contribute less than 10% throughout the entire  $k_T$  range. To reject ghost pairs, only one shared hit out of six in the weak-field region and two shared hits out of five in the strong-field region were allowed per pair. A two-particle acceptance cut was applied to both data and background; the criterion for pair acceptance was defined by  $\Delta\phi + 2\Delta\theta > 0.05$  rad, where  $\Delta\phi$  and  $\Delta\theta$  are the relative pair separation in azimuthal and polar angle, respectively. In this analysis, events in the most central 15% of the cross section were selected. HIJING was used to relate the fraction of the cross section to  $\langle N_{part} \rangle$ , the mean number of participating nucleons [18]. The average number of participants for these events was estimated to be  $\langle N_{part} \rangle = 310$  (303) at  $\sqrt{s_{NN}} = 200$  (62.4) GeV. About 7.3 (3.3) million  $\pi^+\pi^+$  and 5.5 (3.0) million  $\pi^-\pi^-$  pairs for  $\sqrt{s_{NN}} = 200$  (62.4) GeV survive all cuts including centrality selection.

The event-mixed background is constructed by combining single tracks from randomly selected different events into fake pairs. Events from widely spaced collision vertices may yield a background that cannot reproduce the same phase space as the actual data. This effect is particularly prominent for a small-acceptance detector such as PHOBOS. In this analysis, an ‘‘event class’’ is defined solely by the vertex resolution of the detector. Events were defined as belonging to the same event class if they had vertices within 0.025 cm along the beam axis and 0.05 cm along the vertical and horizontal axes. Background events are only constructed from tracks mixed from the same event class.

Systematic errors (90% C.L.) were determined by changing cuts in two-particle acceptance and single-track azimuthal acceptance, using different random seeds for mixed-event background generation, as well as varying

the event class definition to create background events from pairs with narrower and broader vertex ranges. Additionally, these studies were performed for each individual spectrometer arm and the differences included in the systematic uncertainties.

Because the background is constructed from tracks belonging to different events, it does not *a priori* include multiparticle correlations (apart from a residual effect at the few percent level, which has been corrected following [24, 25]). In order to study the HBT correlation, it is necessary to apply a weight to account for the Coulomb effect. The Coulomb correction can be expressed solely as a function of the invariant relative 4-momentum  $\mathbf{q}_{inv}$ ,

$$F_{R_{inv}}(\mathbf{q}_{inv}) = \frac{F_c(\mathbf{q}_{inv})}{F_{pl}(\mathbf{q}_{inv})} = \frac{\int d\vec{r} |\psi_c(\vec{r})|^2 S(\vec{r})}{\int d\vec{r} |\psi_{pl}(\vec{r})|^2 S(\vec{r})} \quad (3)$$

where  $S(\vec{r})$  is the distribution of the relative separation of the particle pairs at emission,  $R_{inv}$  is the radius parameter conjugate to  $\mathbf{q}_{inv}$ , and  $\psi_c$  and  $\psi_{pl}$  are the Coulomb and plane wave-functions, respectively. A closed-form approximation and numerical interpolation for this relation was derived in [26] for  $\lambda = 1$ .

For variable  $\lambda$  [27],

$$F_{R_{inv}}(\mathbf{q}_{inv}, \lambda) = \frac{(1 - \lambda) + \lambda(1 + e^{-\mathbf{q}_{inv}^2 R_{inv}^2}) F_{R_{inv}}(\mathbf{q}_{inv})}{1 + \lambda e^{-\mathbf{q}_{inv}^2 R_{inv}^2}} \quad (4)$$

This prescription was derived simultaneously and is nearly equivalent to the corrections applied by the CERES [28], STAR [29], and PHENIX experiments [30]; our results showed no significant change using either correction method. The method is applied iteratively, successively fitting distributions of the correlation function  $C(\mathbf{q}_{inv})$  and applying the fit values  $\lambda$  and  $R_{inv}$  to a new  $S(\vec{r})$ . Typically 2 or 3 iterations are sufficient for convergence.

The three-dimensional correlation functions were fit by Eq. (2) using MINUIT and the log-likelihood method. Table I shows the results of the fit for both  $\pi^+\pi^+$  and  $\pi^-\pi^-$ . The data were analyzed in the longitudinal co-moving system (LCMS) frame. In Fig. 2, the Bertsch-Pratt parameters and the ratio  $R_o/R_s$  are presented as a function of  $k_T$  for  $\pi^-\pi^-$  pairs at  $\sqrt{s_{NN}} = 62.4$  GeV and 200 GeV. The 200 GeV data are compared to data from STAR [29] and PHENIX [30]. Not shown are values for  $\lambda$ , which is roughly 0.5, and the cross-term  $R_{ol}^2$ , which is consistent with zero for all  $k_T$  bins. The small vertical acceptance of the PHOBOS detector roughly translates into a small acceptance in  $q_s$ , which is responsible for the large statistical and systematic uncertainties on the value of  $R_s$  at low  $k_T$ . Within errors, the values of  $R_s$  are consistent with a weak dependence on  $k_T$ , while the values of  $R_o$  and  $R_\ell$  decrease rapidly with increasing  $k_T$ . Consequently, the ratio  $R_o/R_s$  decreases from  $1.24 \pm 0.19$  to  $0.77 \pm 0.11$  for  $\langle k_T \rangle$  from 0.2 to 0.7 GeV/c. It should be noted that the STAR and PHENIX data are measured at midrapidity while the PHOBOS data are measured at  $\langle y_{\pi\pi} \rangle = 0.9$ ; additionally, STAR, PHOBOS, and

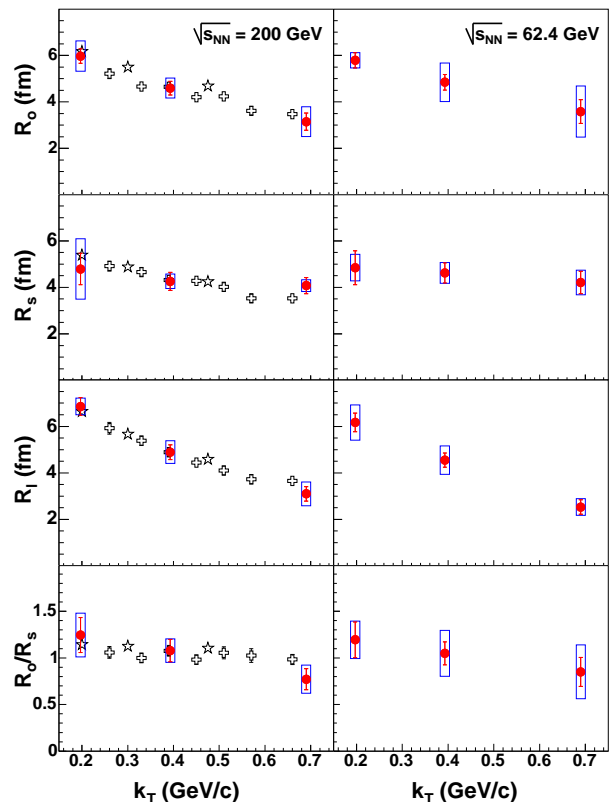


FIG. 2: Bertsch-Pratt parameters  $R_o$ ,  $R_s$ ,  $R_\ell$  and the ratio  $R_o/R_s$  for  $\pi^-\pi^-$  pairs at  $\sqrt{s_{NN}} = 200$  GeV (left panel) and 62.4 GeV (right panel) as a function of  $\langle k_T \rangle$ . For comparison, data from STAR [29] (open stars) and PHENIX [30] (open crosses) are presented at 200 GeV. PHOBOS systematic errors (90% C.L.) are shown as boxes; systematic errors from STAR and PHENIX are not shown.

PHENIX data are from the top 10%, 15%, and 30% of the cross-section respectively.

Despite the very different experimental acceptances, the data at 200 GeV agree remarkably well. The trends at  $\sqrt{s_{NN}} = 62.4$  GeV are qualitatively and quantitatively similar to those at 200 GeV, except that  $R_\ell$  may be slightly smaller.

The Bertsch-Pratt parameters  $\lambda$ ,  $R_o$ ,  $R_s$ , and  $R_\ell$  are presented in Fig. 3 as a function of center of mass energy from  $\sqrt{s_{NN}} = 2$  to 200 GeV. The data are  $\pi^-\pi^-$  pairs near midrapidity for comparable  $k_T$  bins from nine different experiments. The data at  $\sqrt{s_{NN}} = 62.4$  GeV begin to fill the large gap between the top SPS energy and the 130 GeV RHIC data. Although there is some disagreement among experiments, the data do not appear to exhibit any sharp discontinuities, but smoothly vary as a function of collision energy. The correlation function was also fit to the Yano-Koonin-Podgoretskii (YKP) parameterization [31, 32]

$$C(\mathbf{q}) = 1 + \lambda e^{-(q_\perp^2 R_\perp^2 + \gamma^2 (q_{||} - \beta q_\tau)^2 R_\parallel^2 + \gamma^2 (q_\tau - \beta q_{||})^2 R_\tau^2)} \quad (5)$$

where  $\beta$  is the longitudinal velocity of the source and

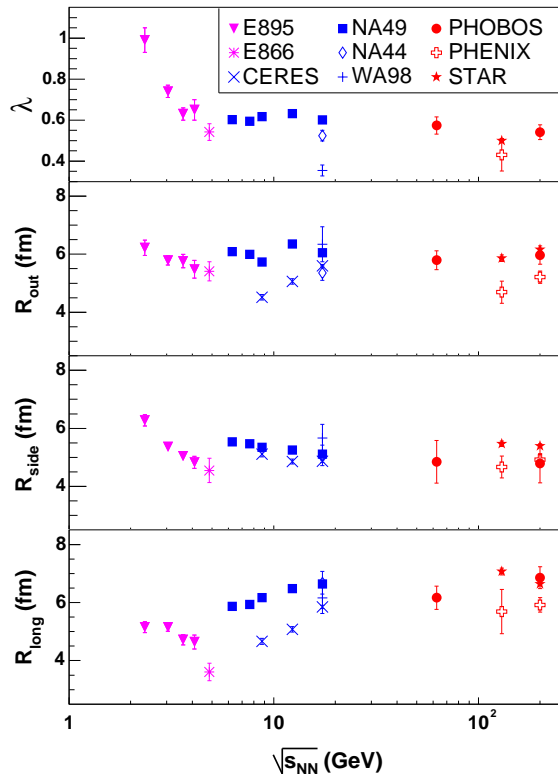


FIG. 3: Bertsch-Pratt parameters  $\lambda$ ,  $R_s$ ,  $R_o$ , and  $R_\ell$  as a function of  $\sqrt{s_{NN}}$  for  $\pi^-\pi^-$  pairs. The presented data are near midrapidity and represent comparable  $k_T$  bins from each experiment [11, 12, 26, 28, 29, 30, 34, 35, 36, 37]. PHOBOS data are represented by solid circles. Systematic errors are not shown.

$\gamma = 1/\sqrt{1-\beta^2}$ ,  $q_\perp$  and  $q_\parallel$  are the relative 3-momentum difference projected in the transverse and longitudinal directions, respectively, and  $q_\tau$  is the relative difference in energy. Employing this coordinate system provides the advantage of factorizing the velocity and duration of the source from the spatial parameters. In addition to fits in the LCMS frame, data were also fit in the laboratory frame as a cross-check and yielded consistent results.

Table II shows the results of Yano-Koonin-Podgoretskii fits for  $\pi^+\pi^+$  and  $\pi^-\pi^-$  at both energies. In Fig. 4, the value of the source rapidity  $y_{YKP}$  (as extracted from  $\beta$  in Eq. 5) is plotted as a function of pair rapidity for  $\pi^-\pi^-$  pairs with  $0.1 < k_T < 1.4$  GeV/c. Open circles indicate the results reflected about midrapidity. The data from NA49 [33] at  $\sqrt{s_{NN}} = 17.2$  GeV is also plotted; however, it should be noted the NA49 data presented here cover only  $0.1 < k_T < 0.2$  GeV/c. The source rapidity scales with the rapidity of the pair, indicating the presence of strong position-momentum

correlations. A static source would exhibit no correlation and would correspond to a horizontal line ( $y_{YKP} = 0$ ). A source with strong dynamical correlations would correspond to a straight line along  $y_{YKP} = y_{\pi\pi}$ . The data

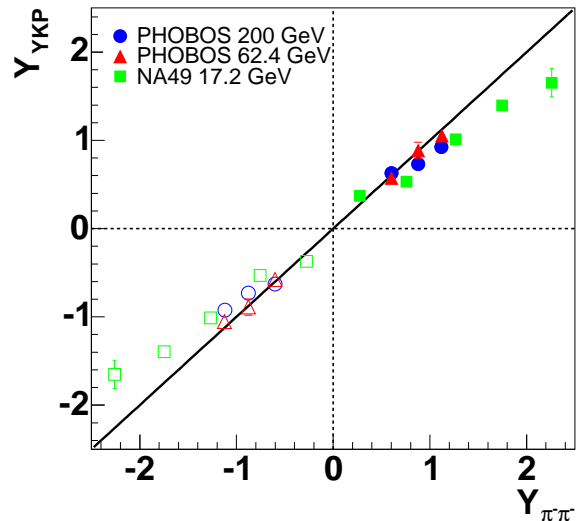


FIG. 4: Dependence of the source rapidity  $y_{YKP}$  vs. the pair rapidity  $y_{\pi\pi}$  for PHOBOS at 200 GeV (circles), PHOBOS at 62.4 GeV (triangles), and NA49 (negatively charged hadrons) at 17.2 GeV [33] (squares). Open symbols represent data reflected about midrapidity.

are consistent with the latter scenario: particles emitted at a given rapidity were produced by a source moving collectively at the same rapidity. In conclusion, we have measured HBT parameters in Au+Au collisions with the PHOBOS detector using both the Bertsch-Pratt and Yano-Koonin-Podgoretskii parameterizations at energies of  $\sqrt{s_{NN}} = 62.4$  GeV and 200 GeV. The ratio  $R_o/R_s$  does not show significant deviation from unity over the entire  $k_T$  range. The data at 200 GeV show a nice agreement between three RHIC experiments with different acceptances, centrality measures, and rapidity, which implies that the source parameters are fairly insensitive to these variables at this energy. Additionally, the Bertsch-Pratt parameters evolve smoothly as a function of  $\sqrt{s_{NN}}$  over nearly two orders of magnitude.

This work was partially supported by U.S. DOE grants DE-AC02-98CH10886, DE-FG02-93ER40802, DE-FC02-94ER40818, DE-FG02-94ER40865, DE-FG02-99ER41099, and W-31-109-ENG-38, by U.S. NSF grants 9603486, 0072204, and 0245011, by Polish KBN grant 1-PO3B-062-27(2004-2007), and by NSC of Taiwan Contract NSC 89-2112-M-008-024.

[1] B. B. Back *et al.*, Phys. Rev. Lett. **91**, 072302 (2003).

[2] S. S. Adler *et al.*, Phys. Rev. Lett. **91**, 072303 (2003).

TABLE I: Bertsch-Pratt fit parameters for  $\pi^+\pi^+$  and  $\pi^-\pi^-$  in the rapidity range  $0.4 < y_{\pi\pi} < 1.3$  for the 15% most central Au+Au collisions. Momenta are in GeV/c and radii are in fm. Errors are statistical ( $1\sigma$ ) followed by systematic (90% C.L.)

Species	$\sqrt{s_{NN}}$	$\langle k_T \rangle$	$\lambda$	$R_o$	$R_s$	$R_t$	$R_{ol}^2$ (fm <sup>2</sup> )
$\pi^+\pi^+$	62.4 GeV	0.198	0.620±0.046±0.075	5.65 ± 0.33 ± 0.44	5.11 ± 0.69 ± 0.61	6.70±0.44±0.63	1.9 ± 2.9 ± 2.6
		0.392	0.660±0.055±0.069	4.72 ± 0.34 ± 0.48	4.74 ± 0.45 ± 0.42	4.53±0.31±0.31	0.85 ± 1.7 ± 2.2
		0.680	0.413±0.073±0.083	2.70 ± 0.60 ± 0.66	3.94 ± 0.46 ± 0.67	2.21 ± 0.52 ± 1.3	0.26±0.91±0.91
$\pi^-\pi^-$	62.4 GeV	0.198	0.574±0.042±0.057	5.79 ± 0.33 ± 0.33	4.85 ± 0.73 ± 0.57	6.17±0.40±0.76	2.2 ± 2.9 ± 2.9
		0.391	0.688±0.059±0.070	4.84 ± 0.34 ± 0.83	4.62 ± 0.44 ± 0.45	4.55±0.31±0.61	0.33 ± 1.9 ± 1.4
		0.673	0.532±0.075±0.13	3.58 ± 0.51 ± 1.1	4.21 ± 0.48 ± 0.53	2.53±0.32±0.36	-0.32 ± 1.2 ± 2.0
$\pi^+\pi^+$	200 GeV	0.198	0.493±0.028±0.041	5.48 ± 0.27 ± 0.36	4.09 ± 0.63 ± 0.66	6.75±0.33±0.26	4.9 ± 2.3 ± 5.7
		0.393	0.582±0.041±0.086	5.05 ± 0.28 ± 0.40	4.64 ± 0.39 ± 0.40	4.75±0.25±0.52	0.96 ± 1.7 ± 2.0
		0.685	0.444±0.049±0.082	3.31 ± 0.32 ± 0.52	3.96 ± 0.36 ± 0.20	2.98±0.29±0.37	0.25 ± 1.1 ± 1.5
$\pi^-\pi^-$	200 GeV	0.198	0.541±0.036±0.048	5.97 ± 0.31 ± 0.65	4.79 ± 0.67 ± 1.3	6.86±0.38±0.36	5.7 ± 3.0 ± 2.2
		0.393	0.559±0.044±0.054	4.59 ± 0.30 ± 0.43	4.26 ± 0.39 ± 0.31	4.89±0.32±0.49	1.1 ± 1.9 ± 3.0
		0.690	0.469±0.055±0.060	3.15 ± 0.37 ± 0.64	4.08 ± 0.35 ± 0.25	3.10±0.31±0.51	0.93 ± 1.1 ± 2.1

TABLE II: Yano-Koonin-Podgoretskii fit parameters for  $\pi^+\pi^+$  and  $\pi^-\pi^-$  in the  $k_T$  range  $0.1 < k_T < 1.4$  GeV/c for the 15% most central Au+Au collisions. Radii are in fm. Errors are statistical ( $1\sigma$ ) followed by systematic (90% C.L.)

Species	$\sqrt{s_{NN}}$	$\langle y_{\pi\pi} \rangle$	$\lambda$	$R_{\perp}$	$R_{\parallel}$	$R_{\tau}$	$\beta$
$\pi^+\pi^+$	62.4 GeV	0.602	0.669±0.057±0.074	5.05 ± 0.33 ± 0.30	5.75 ± 0.45 ± 0.70	0.0017±2.0±1.4	-0.162±0.086±0.11
		0.879	0.512±0.051±0.10	4.21 ± 0.62 ± 0.52	4.88 ± 0.44 ± 0.48	3.7 ± 1.3 ± 3.0	0.119±0.095±0.091
		1.124	0.506±0.046±0.062	3.96 ± 0.42 ± 0.41	5.20 ± 0.47 ± 0.58	3.0 ± 1.0 ± 2.0	-0.0738±0.080±0.082
$\pi^-\pi^-$	62.4 GeV	0.602	0.596±0.055±0.067	4.40 ± 0.70 ± 1.0	5.07 ± 0.44 ± 0.41	4.3 ± 1.2 ± 1.3	-0.0266±0.079±0.098
		0.878	0.539±0.054±0.080	4.78 ± 0.64 ± 0.69	5.10 ± 0.48 ± 0.82	0.75 ± 6.4 ± 2.6	0.0105±0.13±0.23
		1.124	0.525±0.044±0.040	4.09 ± 0.44 ± 0.47	4.84 ± 0.35 ± 0.25	3.3 ± 0.99 ± 2.0	-0.0687±0.075±0.048
$\pi^+\pi^+$	200 GeV	0.602	0.507±0.037±0.056	4.83 ± 0.53 ± 0.48	5.54 ± 0.37 ± 0.36	2.3 ± 1.7 ± 2.3	-0.0967±0.077±0.087
		0.878	0.441±0.034±0.088	4.36 ± 0.53 ± 0.73	5.37 ± 0.37 ± 0.82	1.3 ± 2.9 ± 2.2	-0.130±0.091±0.23
		1.119	0.454±0.031±0.032	3.89 ± 0.37 ± 0.59	5.03 ± 0.31 ± 0.43	3.6 ± 0.70 ± 1.0	-0.115±0.058±0.069
$\pi^-\pi^-$	200 GeV	0.602	0.492±0.040±0.042	3.83 ± 0.55 ± 0.44	5.43 ± 0.38 ± 0.45	4.4 ± 0.96 ± 1.3	0.0270±0.070±0.056
		0.877	0.485±0.042±0.079	4.50 ± 0.50 ± 0.70	5.23 ± 0.40 ± 0.71	2.3 ± 1.6 ± 1.7	-0.146±0.090±0.14
		1.122	0.469±0.040±0.044	4.16 ± 0.44 ± 0.31	5.72 ± 0.43 ± 0.57	2.2 ± 1.3 ± 0.90	-0.193±0.080±0.11

- [3] J. Adams *et al.*, Phys. Rev. Lett. **91**, 072304 (2003).  
[4] I. Arsene *et al.*, Phys. Rev. Lett. **91**, 072305 (2003).  
[5] S. Pratt, Phys. Rev. Lett. **53**, 1219 (1984).  
[6] S. Pratt, Phys. Rev. D **33**, 1314 (1986).  
[7] G. Bertsch, Nucl. Phys. **A498**, 173 (1989).  
[8] S. Chapman, P. Scotto and U. Heinz, Phys. Rev. Lett. **74**, 4400 (1995).  
[9] D. H. Rischke and M. Gyulassy, Nucl. Phys. **A608**, 479 (1996).  
[10] S. Soff, S. A. Bass and A. Dumitru, Phys. Rev. Lett. **86**, 3981 (2001).  
[11] C. Adler *et al.*, Phys. Rev. Lett. **87**, 082301 (2001).  
[12] K. Adcox *et al.*, Phys. Rev. Lett. **88**, 192302 (2002).  
[13] K. Morita and S. Muroya, Prog. Theor. Phys. **111**, 93 (2004).  
[14] M. Csanád *et al.*, nucl-th/0403074.  
[15] F. Retière and M. A. Lisa, nucl-th/0312024.  
[16] T. Renk, Phys. Rev. C **69**, 044902 (2004).  
[17] B. B. Back *et al.*, Nucl. Inst. Meth. **A499**, 603 (2003).  
[18] B. B. Back *et al.*, Phys. Rev. Lett. **85**, 3100 (2000).  
[19] B. B. Back *et al.*, Nucl. Phys. **A698**, 555 (2002).  
[20] B. B. Back *et al.*, Phys. Rev. Lett. **87**, 102301 (2001).  
[21] B. B. Back *et al.*, Phys. Lett. **B578**, 297 (2004).  
[22] M. Gyulassy and X. N. Wang, Comput. Phys. Commun.

- 83**, 307 (1994).
- [23] GEANT 3.2.1, CERN program library.
  - [24] W. Zajc *et al.*, Phys. Rev. C **29**, 2173 (1984).
  - [25] V. Cianciolo, Ph. D. thesis, M.I.T. (1994).
  - [26] L. Ahle *et al.*, Phys. Rev. C **66**, 054906 (2002).
  - [27] B. Holzman *et al.*, nucl-ex/0406027.
  - [28] D. Adamová *et al.*, Nucl. Phys. **A714**, 124 (2003).
  - [29] J. Adams *et al.*, Phys. Rev. Lett. **93**, 012301 (2004).
  - [30] S. S. Adler *et al.*, nucl-ex/0401003.
  - [31] F. Yano and S. Koonin, Phys. Lett. **B78**, 556 (1978).
  - [32] M. Podgoretskii, Sov. J. Nucl. Phys. **37**, 272 (1983).
  - [33] H. Appelshäuser *et al.*, Eur. Phys. J. **C2**, 661 (1998).
  - [34] M. A. Lisa *et al.*, Phys. Rev. Lett. **84**, 2798 (2000).
  - [35] I. G. Bearden *et al.*, Phys. Rev. C **58**, 1656 (1998).
  - [36] S. Kniege *et al.*, nucl-ex/0403034.
  - [37] M. M. Aggarwal *et al.*, Eur. Phys. J. **C16**, 445 (2000).